Electron and Negative Ion Densities in C_2F_6 and CHF_3 containing Inductively Coupled Discharges

G. A. Hebner and P. A. Miller

Sandia National Laboratories, Albuquerque NM, 87185-1423

Abstract

Electron and negative ion densities have been measured in inductively coupled discharges containing C_2F_6 and CHF_3. Line integrated electron density was determined using a microwave interferometer, negative ion densities were inferred using laser photodetachment spectroscopy, and electron temperature was determined using a Langmuir probe. For the range of induction powers, pressures and bias power investigated, the electron density peaked at 9×10^{12} cm^{-2} (line-integrated) or approximately 9×10^{11} cm^{-3}. The negative ion density peaked at approximately 1.3×10^{11} cm^{-3}. A maximum in the negative ion density as a function of induction coil power was observed. The maximum is attributed to a power dependent change in the density of one or more of the potential negative ion precursor species since the electron temperature did not depend strongly on power. The variation of photodetachment with laser wavelength indicated that the dominant negative ion was F^-. Measurement of the decay of the negative ion density in the afterglow of a pulse modulated discharge was used to determine the ion-ion recombination rate for CF_4, C_2F_6 and CHF_3 discharges.

DISCLAIMER

I. Introduction

Discharges containing fluorocarbon gases such as C_2F_6 and CHF_3 are commonly used to etch silicon dioxide for microelectronic feature definition. These gases serve as rich sources of atomic fluorine to remove the silicon dioxide as well as $C_xH_yF_z$ radicals that provide sidewall passivation and protection. While high electron density plasmas such as inductively coupled plasmas (ICP) and electron cyclotron resonance (ECR) microwave driven plasmas are commonly used for metal line definition, their use with fluorocarbon gases is problematic. In metal etch systems, the high degree of precursor gas dissociation (usually Cl bearing species) greatly increases etch rate and chamber through put. However, anisotropic oxide etching has been shown to result from a critical balance between etching due to atomic fluorine, and sidewall and photoresist protection due to $C_xH_yF_z$ radicals depositing on the surface. In most high density systems, it is very easy to excessively dissociate the $C_xH_yF_z$ species and generate a fluorine rich environment that is detrimental to a stable, anisotropic oxide etch process. In addition to standard silicon and oxide etch processing applications, recent advances in the processing of low dielectric materials (low-k) suggest that small additions of fluorocarbon gases to produce $C_xH_yF_z$ radicals for surface and sidewall protection and passivation may be critical to anisotropic etching of these next-generation materials. Thus there is a need to understand the gas and surface phase chemistry in high density plasma systems in order to exploit fully the potential of high density plasmas for stable, high throughput processes.

In electronegative plasma systems, such as fluorocarbon discharges, it is important to determine both the electron and negative ion density. Due to their high

mass, the negative ions can strongly influence the sheath voltage and kinetics, and in the case of pulsed discharge systems, possibly influence the surface charge. Additionally, negative ion formation serves as a loss mechanism for electrons, and since negative ions tend to collect in regions of maximum plasma potential, they can serve as a significant loss term for volumetric ion-ion recombination of positive ions.

Unfortunately, characterization of the charged particle density in fluorocarbon discharges is complicated by the formation of stable plasma radicals that can quickly coat *in-situ* diagnostic probes with an insulating layer. To circumvent this problem, a number of techniques have been used. In the case of Langmuir probes, a myriad of different techniques have been proposed or attempted. In cases where the deposition rate is not very fast, it is possible to sweep the probe voltage quickly, to put a high negative bias on the probe to ion-sputter clean the probe tip, or to electrically heat the probe tip.[1,2,3,4,5] For example, Takada et al[4] and Maeda et al[5] have demonstrated the use of hot probes to measure the negative ion density in CF_4 and Ar / O_2 containing plasmas, respectively. However, in most cases, the lifetime of hot probes in fluorine containing plasmas is severely limited. Alternative approaches include the work of Braithwaite et al who demonstrated a novel electrostatic probe based upon the discharge rate of the rf biased probe capacitance.[6] The probe can be used to determine the ion flux even in the presence of insulating layers. St-Onge et al also recently demonstrated a novel technique in SF_6 / Ar plasmas to characterize the positive to negative ion ratio based upon a measurement of the velocity of ion acoustic waves.[7]

There are also methods of investigating the plasma charged particle density that do not involve probes. For example, it is possible to use mass spectrometer systems to

monitor the positive ion flux.[8,9] While there are notable exceptions,[10] in most cases, such systems are fairly large and can only be used to monitor the flux at the chamber wall; they do not provide spatial or temporal resolution. Alternatively, in depositing plasmas, microwave based diagnostics have an advantage in that they do not contact the plasma. The main disadvantage is that one generally needs line of sight access to the plasma and the window deposition rate can not be excessive. Microwave diagnostics have been shown to have sufficient time resolution to enable laser photodetachment measurements of the negative ion density. For example, Haverlag et al have measured the negative ion density in CF_4, C_2F_6, CHF_3 and C_3F_8 discharges.[11] By scanning the laser wavelength, they showed that for low power, parallel plate discharges, the dominant negative ion, F^- or CF_3^-, depends on the precursor gas.

The goal of this investigation was to determine the electron and negative ion density in inductively coupled, high electron density plasmas. The data will be used to determine the electron to negative-ion density ratio, to begin to investigate the negative ion formation mechanisms, to identify the dominant negative ion, and to provide data to validate models. For this work, we used a microwave interferometer to measure the line integrated electron density and negative ion density. In the course of these experiments, we also used a Langmuir probe to provide an indication in the trends of the electron temperature.

II. Experimental Configuration

Experiments were performed in a Gaseous Electronics Conference (GEC) rf reference cell which was modified to include an inductively coupled plasma (ICP)

source.[1,12] As shown in Fig. 1, the induction coil was constructed from 3.2 mm diameter copper tubing which was wound into a five-turn planar coil 11 cm in diameter, and was water cooled. In this work, the coil was excited at 13.56 MHz. The coil was separated from the plasma by a 1-cm-thick fused silica window. The spacing between the window and the grounded lower electrode was 3.8 cm. For these experiments, the lower electrode was rf biased (13.56 MHz) and covered with a 6 inch diameter silicon wafer which was not clamped in place. The lower electrode was water cooled; however, the reactor was run with a discharge ($C_xH_yF_z$ or O_2) for 30 minutes to reach a steady-state temperature before any measurements were made. For these experiments an additional modification was made to the GEC chamber; a fused silica ring was clamped to the upper electrode assembly as shown in Fig. 1. The fused silica confinement ring served to stabilize and extend the operating parameter space of the fluorocarbon discharges. Without the ring in place, the discharge could only be sustained over a narrow range of power and pressure. The ring had an inner diameter of 4.5 inches, outer diameter of 6.5 inches and a thickness of 0.75 inches. In addition, the standard stainless steel ICP window holder was replaced by an anodized aluminum holder so that the materials in contact with the plasma would more closely resemble those found in commercial tools.

Line integrated electron density was measured using a microwave interferometer, while the negative ion density was inferred from a laser photodetachment measurement. The equipment and experimental configuration were identical to that described in previous studies of the electron and negative ion density in Cl_2 and BCl_3 containing inductive discharges.[13,14] The microwave interferometer operated at 80 GHz, and standard, high gain horns and microwave lenses were used to transmit the microwaves

through the plasma. The majority of the photodetachment experiments were performed using a frequency-shifted Nd:YAG laser with typical pulse energy of 20 mJ at 266 nm and 100 mJ at 355 nm. To convert the measured excess electron density produced by photodetachment to an absolute negative ion density, several calibration factors must be utilized. First, the spatial distribution of the microwave probe beam must be determined. Second, the spatial energy distribution of the photodetaching laser should be made uniform or be measured. Third, a fractional photodissociation efficiency must be calculated from the measured cross section; any given photon that traverses the plasma may not photodetach an electron from a negative ion.[15,16] For the laser energy used in this experiment, approximately 10 - 30 percent of the F^- was photodetached and the excess electron density was linear in laser energy. Finally, the microwave interferometer and amplifiers must be calibrated. The total uncertainty of these calibrations results in a factor of two uncertainty in the absolute F^- number density. However, in any given data set (one plot), the *relative* density variation was reproducibly $\pm$10 percent. Measurements made at 266 nm and 355 nm yielded the same values for the negative ion density, to within the uncertainty in the photodetachment cross sections.

Since previous work suggested that both F^- and CF_3^- might be present in some fluorocarbon the discharges,[11] several different experiments were conducted to identify the negative ion in the inductively excited discharge. First, measurements performed at 266 nm and 355 nm yielded the same value for the negative ion density (assuming it is F^-), to within the uncertainty of the absolute F^- photodetachment cross sections.[16] However, the relatively large uncertainty in the cross section at 355 nm makes it difficult to set a very small upper bound on the presence of other negative ions. To address this

problem, a tunable pulsed laser (Continuum Sunlite) was used to measure the excess electron density at 300 and 380 nm; above and below the F^- photodetachment threshold of approximately 365 nm. While the absolute photodetachment cross section for CF_3^- is not known, the relative photodetachment cross section decreases by approximately a factor of 3 as the wavelength is varied from 300 to 380 nm.[17] Photodetachment measurements in C_2F_6, CHF_3 and CF_4 plasmas operated at 200 W and 10 mTorr indicated that the excess electron density generated at 380 nm was less than 2 percent of the value at 300 nm. Assuming that the unknown photodetachment cross section for CF_3^- is on the order of F^-, CF_3^- does not appear to have a significant density in these discharges and F^- is the dominant negative ion.

The electron temperature and density were measured with a single Langmuir probe using techniques similar to those described previously.[1] The measured probe characteristics were fitted to a Maxwellian distribution in the range from approximately 1 to 10 eV. Consequently, the reported temperatures correspond to bulk temperatures and do not include information on either very low- or high-energy electrons. To reduce problems with polymer deposition, the probe was biased negatively (e.g. -50 V) and pulsed positively only for short periods of time (<2 ms) at a 20-50 Hz rate. Consequently, the probe was subjected to strong ion bombardment for the majority of its operational use. During the brief positive pulses (ramped V), the probe V-I characteristics were recorded and averaged using transient digitizers. Tuned probe circuits allowed the probe to follow the rf oscillations in plasma potential. To further reduce polymer-deposition problems with the probe, an oxygen discharge was operated for 1 minute to clean the chamber, then the fluorocarbon discharge was operated for 1

minute to obtain a single measurement and then oxygen again used for 1 minute to clean. By alternating between oxygen and the fluorocarbon gas, we found we could obtain reproducible data. While we do not show the electron density derived from the probe, the numbers are is good agreement (30 percent) with values from the microwave interferometer. Using the spatial distributions obtained from the Langmuir probe, the line integrated number density can be converted to a peak density in the center of the plasma by dividing the plotted line integrated density by 10 cm.

The rf voltage and current (zero-to-peak values) for the induction coil are shown in Fig. 2 as functions of input power, and in Fig. 3 as functions of reactor pressure for two representative gas mixtures. Total input power was the difference between the forward and reflected rf power measured by a wattmeter placed between the amplifier and the matching network. For all measurements reported here, the reflected power was less than 2 W. Plasma power is the difference between the total input power and the power dissipated resistively in the coil circuit. For a typical coil resistance of 0.5 Ω, approximately 80% of the total input power was deposited in the plasma. Bias voltage and current at the lower electrode are shown in Fig. 4 as functions of the bias power. The method to analyze the harmonic content of the waveforms has been previously discussed.[1,12] In all cases, the voltage and current for harmonics higher than the second were negligible. There are some significant differences in the harmonic content for the two gases, possibly related to the differences in the electron density.

III. Results and Discussion

Electron and negative ion density in C_2F_6 and CHF_3 and electron temperature in C_2F_6 as functions of the inductive power are shown in Fig. 5. The pressure was constant at 10 mTorr and the wafer bias power was 20 W. The electron density increased linearly with power and was approximately independent of gas. The linear increase with power has also been observed in a number of other gases in the GEC chamber.[14] While the absolute negative ion number density was lower in CHF_3 than C_2F_6, both gases had a maximum in negative ion density at a power of approximately 250 W. Below 250 W, the negative ion density increased linearly with power and electron density. Since the electron density increased linearly with rf power, a linear increase in negative ion density would be expected if the negative ion formation process is dissociative attachment ($XY + e^- \rightarrow X^- + Y$) and the concentration of the precursor species (XY) did not vary with power. However, for induction coil powers above 250 W, the negative ion density decreased with power, despite an increase in electron density.

The measured decrease in the negative ion density for powers above 250 W could be due to a number of different processes. Most negative ion formation rates strongly depend on electron temperature; most negative ion formation processes favor low energy electrons ($E_e < 1$ eV). Thus a change in electron temperature can lead to changes in the negative ion formation rate. Since the measured electron temperature was approximately constant over the range that it was measured, the strong decrease in negative ion density for powers above 250 W does not appear to be due to changes in the electron temperature. However, while the measured electron temperature did not change over the range of interest, the Langmuir probe did not sample the low energy tail ($E_e < 1$ eV) of the electron energy distribution function (EEDF). Thus we can not rule out changes in

the EEDF. In addition, a change in the density of the precursor molecular species (XY) due to electron driven dissociation would reduce the negative ion density formation rate. However, recent laser induced fluorescence measurements of the CF and CF_2 density in these discharges indicate that the CF and CF_2 density do not change strongly for these plasma conditions.[18] Thus some other molecular precursor may be the source of the negative ion. In addition to processes that modify the formation rate, the decrease could be due to changes in the negative ion loss rate due to volumetric recombination. However, since the electron density is an order of magnitude higher than the negative ion density, the total positive ion density also increased linearly with rf power. Thus, for the volumetric recombination rate to change, the dominant positive ion would need to change with increased rf power. This particular possibility appears to be ruled out by recent mass spectrometry measurements for these plasma conditions that indicates that the dominant positive ion does not change with rf power.[8]

Electron and negative ion density in C_2F_6 and CHF_3, and electron temperature in C_2F_6 as functions of pressure are shown in Fig. 6. The induction coil power was constant at 200 W and the wafer bias power was 20 W. As the pressure was increased from 5 to 35 mTorr, the electron density deceased by a factor of two in C_2F_6 and was approximately constant in CHF_3. Despite the constant or decreasing electron density, the negative ion density increased slightly for pressures of 5 – 10 mTorr and was relatively constant above 10 mTorr. In Cl_2 and BCl_3, an increase in the pressure resulted in an increase in the negative ion density.[13,14] This would be expected if the density of the XY species increased with pressure. While there is some evidence that this happens at lower pressures, for pressures above 10 mTorr, there appears to be a rough balance between

electron driven production (from the feed gas or one of its dissociation products) and recombination losses. Over this pressure range, the electron temperature showed a significant decrease from approximately 7.8 to 4 eV. This relatively large change in electron temperature did not appear to have an associated impact on the negative ion density; a large decrease in electron temperature would normally be expected to result in an increase in negative ion density, all other factors being constant. Thus the negative ion formation rate does not appear to be a strong function of electron temperature, or at least the fraction of the EEDF sampled by the probe. Since an almost factor of two change in the electron temperature had no obvious impact on the negative ion density, it appears unlikely that the decrease in negative ion density with rf power discussed above is due to electron temperature effects but rather is driven by production or loss mechanisms.

Electron and negative ion density in C_2F_6 and CHF_3 and electron temperature in C_2F_6 as functions of rf bias power are shown in Fig. 7. The induction coil power was constant at 200 W and the pressure was 10 mTorr. For rf bias powers below approximately 60 W, changes in the rf bias power had no influence on the electron density or the negative ion density despite an increase in the electron temperature. This observation is consistent with a number of other measurements that showed that the presence of a rf wafer bias had minimal influence on the plasma parameters. However, for rf bias powers above 60 W, there was a transition to a slightly higher electron density and a significant decrease in the negative ion density. The increase in electron density and decrease in negative ion density may be due to the rf biased electrode increasing the net power into the plasma and modifying the gas phase chemistry. As discussed above,

for induction coil powers above 250 W, the electron density increased and the negative ion density changed slope and decreased. As the bias power was increased above 60 W, it is likely to be adding power into the plasma as well as accelerating the ions, albeit via a significantly different power deposition mechanism than the ICP coil. This implies that models of these gases should include power deposition due to a number of possible mechanisms.

Since the negative ions are usually confined to the bulk of the plasma by the plasma potential, their dominant loss mechanism is ion-ion recombination. Conversely, the negative ion serves as a loss mechanism for positive ions in the bulk plasma. While the ion-ion recombination rate has been measured in CF_4, it has not been measured in C_2F_6 or CHF_3. Thus, the ion-ion recombination rate was measured for C_2F_6, CHF_3 and CF_4. The measurements were performed by pulse modulating the induction coil power and measuring the decrease in the negative ion density in the afterglow. The experimental system was similar to that used for measurements in pulse modulated Cl_2 discharges.[19] After waiting 10 μsec for the electron density to decay several orders of magnitude to insure a negative ion – positive ion plasma, the time dependent negative ion density was fit to a single decay curve to determine the ion – ion recombination rate. An example is shown in Fig. 8 for CHF_3. The measured ion-ion recombination rate was 0.88 x 10^{-6}, 1.5 x 10^{-6} and 3.9 x 10^{-6} cm^3/s in CF_4, C_2F_6 and CHF_3 respectively. Our value for CF_4 is in good agreement with the previous measured value of 0.6 x 10^{-6} by Haverlag et al[11] but is higher than the value of 0.17 x 10^{-6} measured by Takada.[4] While the negative ion in all cases was F^-, the dominant positive ion is different for each gas, leading to different ion-ion recombination rates. For the case of C_2F_6, the dominant ion was CF_3^+

and in CHF_3 it was CF_2^+.[8] However, the relative density of other positive ions is also significant so the ion-ion recombination rate is really an amalgam of contributions due to all the positive ions.

IV. Summary

Electron and negative ion densities have been measured in inductively coupled discharges containing C_2F_6 and CHF_3. The dominant negative ion was inferred to be F^- by varying the laser wavelength in photodetachment measurements. For the range of induction powers, pressures and bias power investigated, the electron density peaked at 9 x 10^{12} cm^{-2} (line-averaged) or approximately 9 x 10^{11} cm^{-3}. The negative ion density peaked at approximately 1.3 x 10^{11} cm^{-3}. A maximum in the negative ion density as a function of induction coil power was observed. The maximum is attributed to a power dependent change in the density one or more of the negative ion precursor species. An almost factor of two change in the measured electron temperature had no obvious impact on the negative ion density. Thus it appears unlikely that the negative ion density is strongly influenced by electron temperature effects but rather is driven by changes in the production or loss mechanisms. However, this conclusion is tempered with the caveat that the electron temperature was determined from a fit to the bulk of the electron energy distribution function; the probe does not efficiently sample the low energy electrons. Measurement of the decay of the negative ion density in the afterglow of a pulse modulated discharge was used to determine the ion-ion recombination rate; the measured ion-ion recombination rate was 0.88 x 10^{-6}, 1.5 x 10^{-6} and 3.9 x 10^{-6} cm^3/s in CF_4, C_2F_6 and CHF_3 respectively.

V. Acknowledgments

The authors thank P. Ho and J. Johannes for many helpful discussions. The technical assistance of T. W. Hamilton is gratefully recognized. This work was performed at Sandia National Laboratories and supported by SEMATECH and the United States Department of Energy (DE-AC04-94AL85000).

Figure captions

Fig. 1 Cross section view of the GEC rf reference chamber showing the location of the fused silica confinement ring and rf biased electrode.

Fig. 2 Induction coil voltage, current and coil power loss and total plasma power as functions of the power input into the matching network for C_2F_6 (●) and CHF_3 (▼) discharges. The pressure was 10 mTorr.

Fig. 3 Induction coil voltage, current and coil power loss and total plasma power as functions of the pressure for C_2F_6 (●) and CHF_3 (▼) discharges. The induction coil power was 200 W.

Fig. 4. Bias voltage and current at the wafer surface as functions of the bias power into the lower electrode for C_2F_6 (●) and CHF_3 (▼) discharges. Voltages and currents at both the fundamental (f_o = 13.56 MHz) and the second harmonic ($2f_o$ = 27.12 MHz) are shown.

Fig. 5. Electron and negative ion density in C_2F_6 (●) and CHF_3 (▼) and electron temperature in C_2F_6 as functions of induction coil power. The pressure was 10 mTorr and the rf bias was 20 W.

Fig. 6. Electron and negative ion density in C_2F_6 (●) and CHF_3 (▼) and electron temperature in C_2F_6 as functions of pressure. The induction coil power was 200 W and the rf bias was 20 W.

Fig. 7. Electron and negative ion density in C_2F_6 (●) and CHF_3 (▼) and electron temperature in C_2F_6 as functions of bias power. The induction coil power was 200 W and the pressure was 10 mTorr.

Fig. 8. Measured (●) and fit (line) negative ion density in the afterglow of a pulse modulated CHF_3 discharge. The discharge was turned off at t = 0 s. The peak inductive power was 200 W, pressure was 10 mTorr and the rf bias was zero (grounded).

[1] P. A. Miller, G. A. Hebner, K. E. Greenberg, P. D. Pochan and B. P. Aragon, J. Resch. Natl. Int. Standard. Technol 100, 427 (1995).

[2] B. A. Smith and L. J. Overzet, Rev. Sci. Instrum. 69(3), 1372 (1998).

[3] G. Chiodini, C. Riccardi and M. Fontanesi, Rev. Sci. Instrum. 70(6), 2681 (1999).

[4] N. Takada, D. Hayashi, K. Sasaki and K. Kadota, Jpn. J. Appl. Phys. Vol. 36, pt. 2, 12B, L1702, (1997).

[5] M. Maeda, K. Higuchi and S. Matsumura, Jpn. J. Appl. Phys. Vol 36, pt. 1, 7B, 4656 (1997).

[6] N. Braithwaite, J. P. Booth, G. Cunge, Plasma Sources Sci. Technol. 5(4), 677 (1996).

[7] L. St-Onge, J. Margot and M. Chaker, Appl. Phys. Lett. 72(3), 290 (1998).

[8] R. Prakash, R. T. McGrath and G. A. Hebner, J. Vac. Sci. Technol. A 17(4), 1545 (1999).

[9] J. K. Olthoff and Y. Wang, J. Vac. Sci. Technol A 17(4), 1552 (1999).

[10] M. G. Blain, unpublished.

[11] M. Haverlag, A. Kono, D. Passchier. G. M. W. Kroesen, W. J. Goedheer and F. J. de Hoog, J. Appl. Phys. 70(7), 3472 (1991).

[12] P. J. Hargis Jr., K. E. Greenberg, P. A. Miller, J. B. Gerardo, J. R. Torczynski, M. E. Riley, G. A. Hebner, J. R. Roberts, J. K. Olthoff, J. R. Whetstone, R. J. Van Brunt, M. A. Sobolewski, H. M. Anderson, M. P. Splichal, J. L. Mock, P. Bletzinger, A. Garscadden, R. A. Gottscho, G. Selwyn, M. Dalvie, J. E. Heidenreich, J. W. Butterbaugh, M. L. Brake, M. L. Passow, J. Pender, A. Lujan, M. E. Elta, D. B.

Graves, H. H. Sawin, M. J. Kushner, J. T. Verdeyen, R. Horwath and T. R. Turner, Rev. Sci. Inst. 65, 140 (1994).

[13] G. A. Hebner, J. Vac. Sci. Technol. A. 14(4), 2158 (1996).

[14] C. B. Fleddermann and G. A. Hebner, J. Vac. Sci. Technol. A, 15(4), 1955 (1997).

[15] A. Mandl, Phys. Rev. A, 3(1), 251 (1971).

[16] S. Vacquie, A. Gleizes and M. Sabsabi, Phys. Rev. A, 35(4), 1615 (1987).

[17] J. H. Richardson, L. M. Stephenson and J. I. Brauman, Chem. Phys. Lett. 30(1), 17 (1975).

[18] G. A. Hebner, unpublished.

[19] G. A. Hebner and C. B. Fleddermann, J. Appl. Phys., 82(6), 2814 (1997).

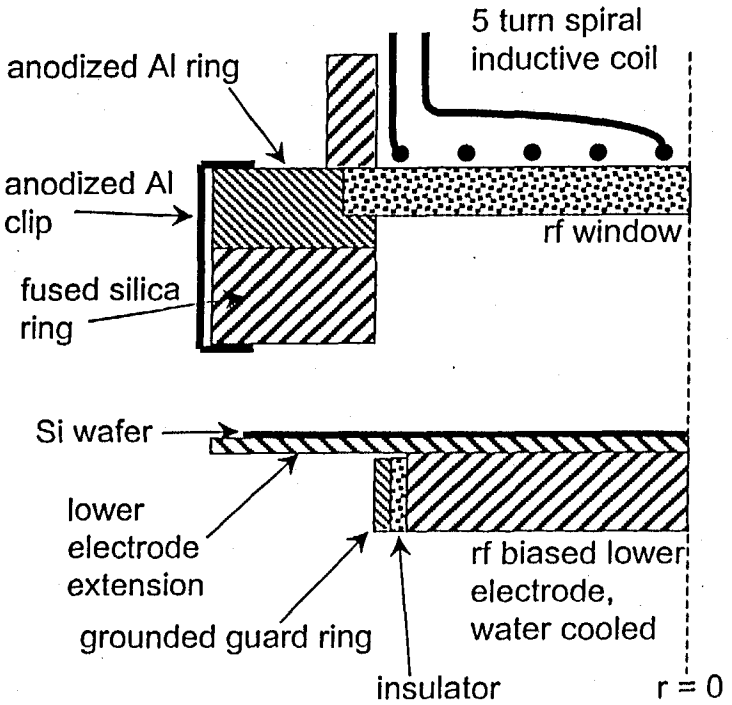
5 turn spiral
inductive coil
anodized Al ring
anodized Al
clip
rf window
fused silica
ring
Si wafer
lower
electrode
extension
rf biased lower
electrode,
water cooled
grounded guard ring
insulator
r = 0

Fig 1
HEBNER

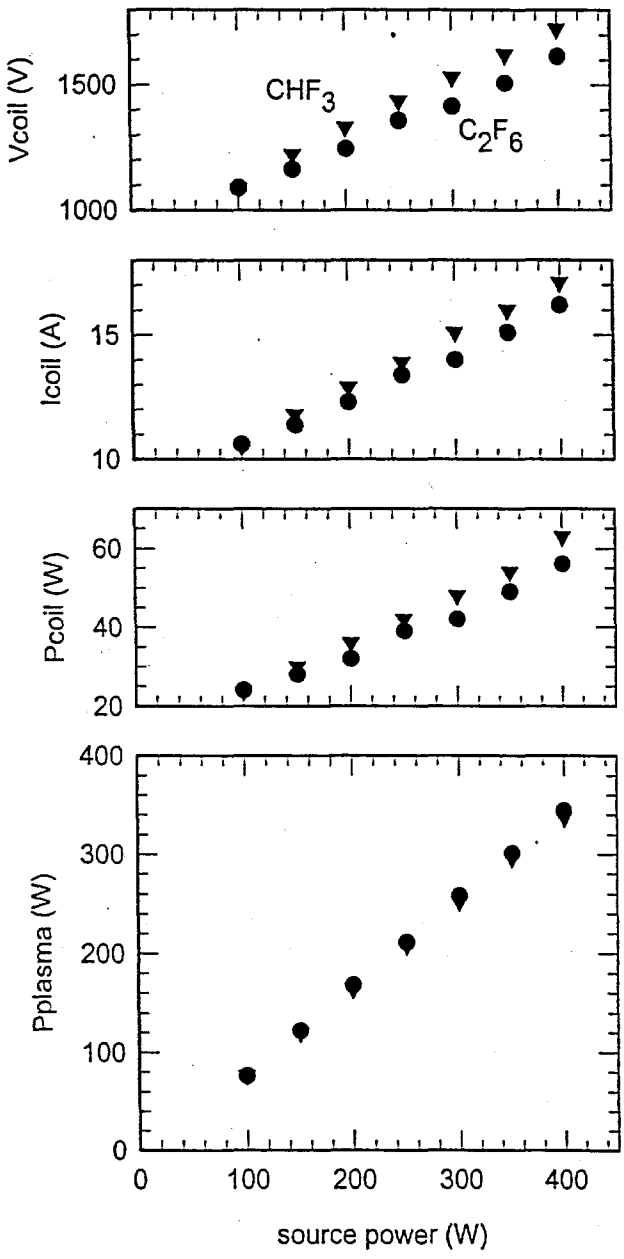
Vcoil (V)
1500
1000
CHF3
C2F6
Icoil (A)
15
10
Pcoil (W)
60
40
20
Pplasma (W)
400
300
200
100
0
0
100
200
300
400
source power (W)

Fig. 2
Hebner

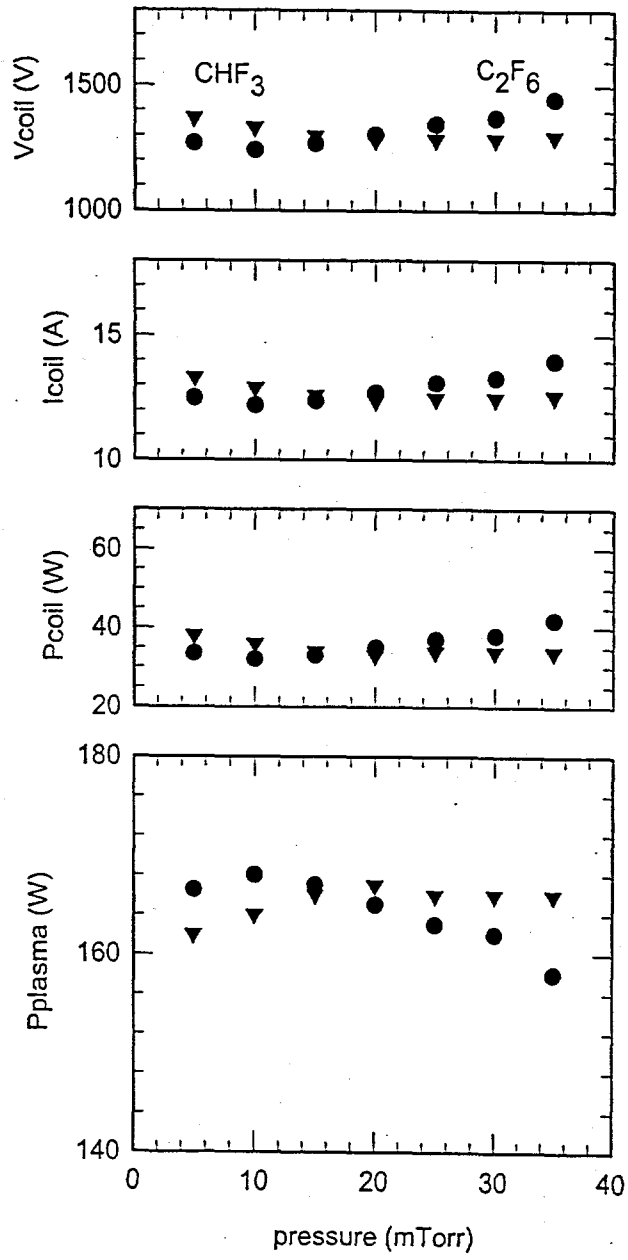
Vcoil (V)
1500
1000
CHF3
C2F6
Icoil (A)
15
10
Pcoil (W)
60
40
20
Pplasma (W)
180
160
140
0
10
20
30
40
pressure (mTorr)

Fig. 3
Hebner

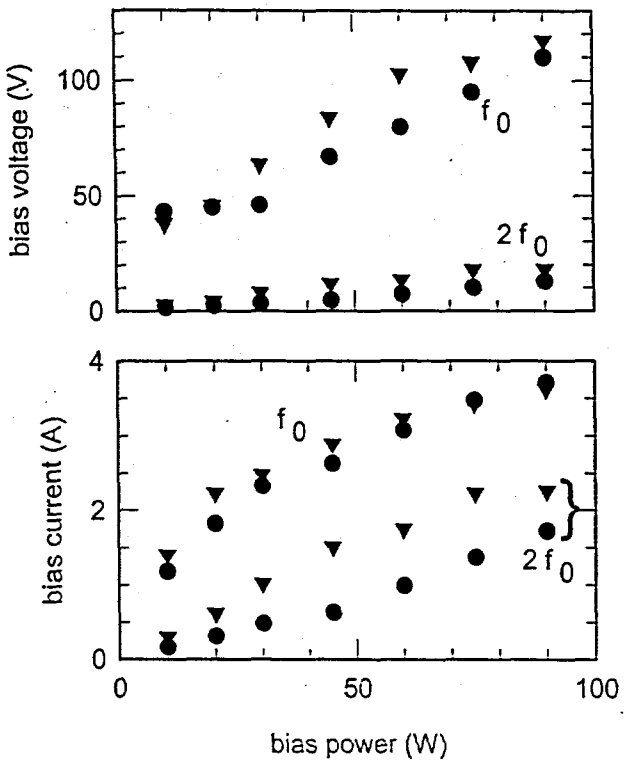
bias voltage (V)
100
50
0
f 0
2 f 0
bias current (A)
4
2
0
f 0
2 f 0
0
50
100
bias power (W)

Fig. 4
Hebner

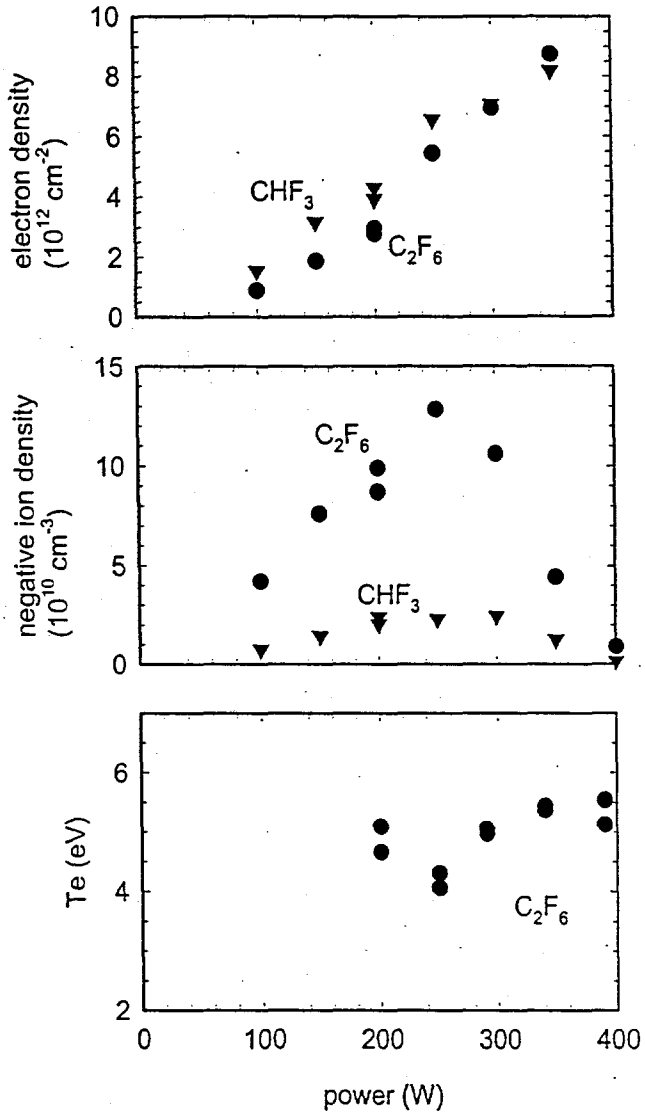
electron density
(10^{12} cm^{-2})
10
8
6
4
2
0
CHF_3
C_2F_6
negative ion density
(10^{10} cm^{-3})
15
10
5
0
C_2F_6
CHF_3
Te (eV)
6
4
2
C_2F_6
0
100
200
300
400
power (W)

Fig. 5
Hebner

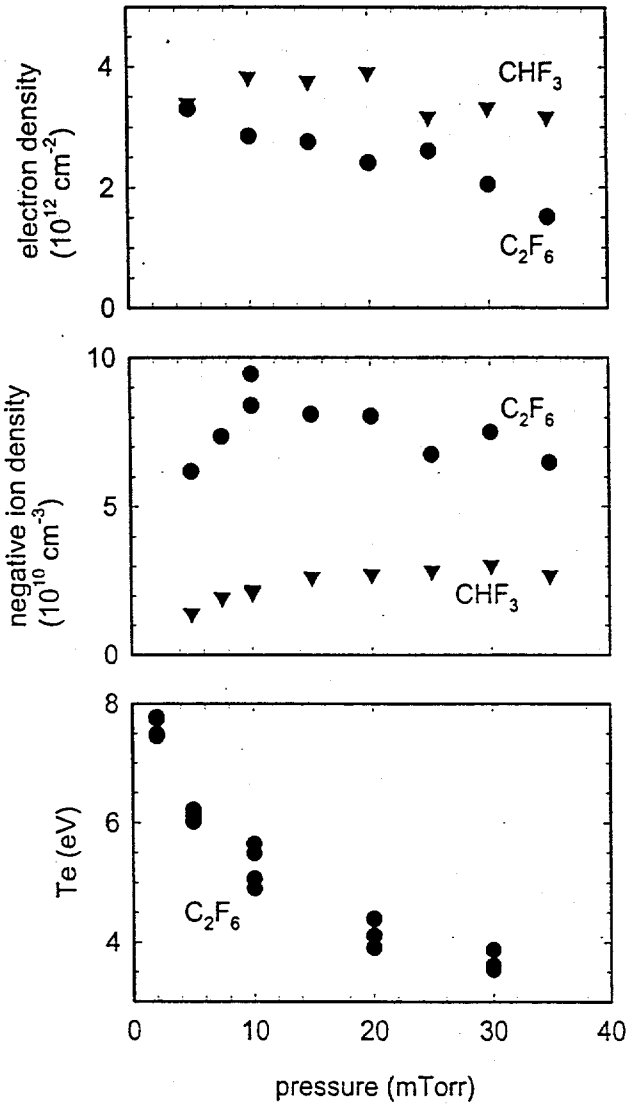
electron density
(10^{12} cm^{-2})
4
2
0
CHF_3
C_2F_6
negative ion density
(10^{10} cm^{-3})
10
5
0
C_2F_6
CHF_3
Te (eV)
8
6
4
C_2F_6
0
10
20
30
40
pressure (mTorr)

Fig. 6
Hebner

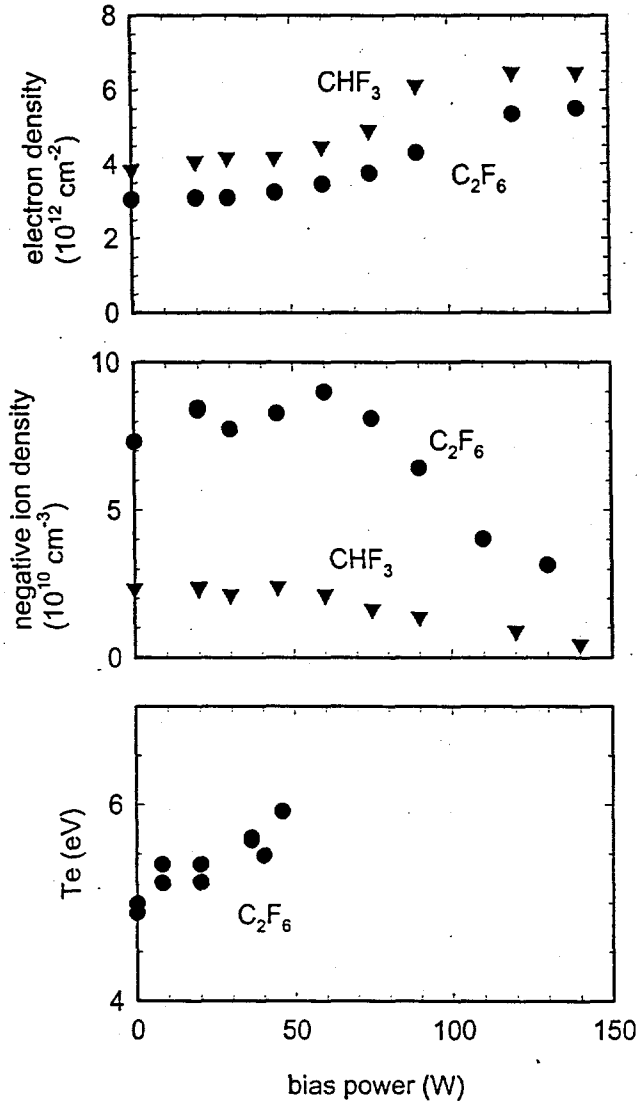
electron density
(10^{12} cm^{-2})
8
6
4
2
0
CHF_3
C_2F_6
negative ion density
(10^{10} cm^{-3})
10
5
0
C_2F_6
CHF_3
Te (eV)
6
4
C_2F_6
0
50
100
150
bias power (W)

Fig. 7
Hebner

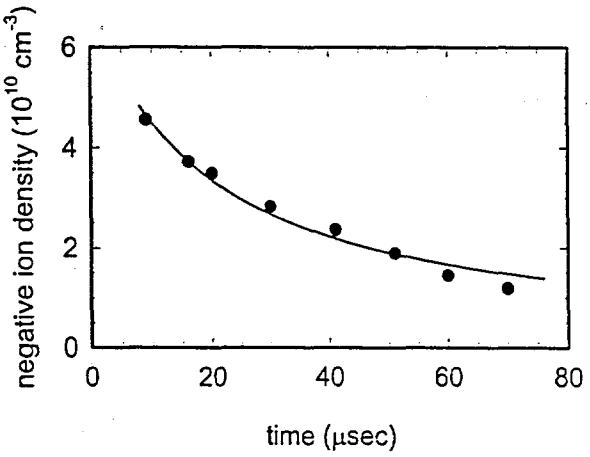

Fig 8
Hebner